



A novel successful strategy for the detection of antibiotics and toxic heavy metals based on fluorescence silver/graphene quantum dots nanocomposites

Amira H. E. Moustafa¹ · Mahmoud A. Mousa² · Hanaa H. Abdelrahman¹ · Mamdouh A. Fahmy³ · Dina G. Ebrahim³

Received: 28 July 2022 / Accepted: 4 July 2023
© King Abdulaziz City for Science and Technology 2023

Abstract

Antibiotic residue and toxic heavy metals in aquaculture have a hazardous impact on human health and environmental safety. So the biggest challenge is designing a powerful detecting tool without harming fisheries and the environment. A novel dual-function silver/graphene quantum dots ($Ag@GQDs$)-based fluorescence nanosensor was developed to investigate unprecedented sensing strategies for sensitive and selective detection of antibiotics and heavy metals to ensure that they are present in the authorized percentage. Here, the fluorescence nanocomposites achieve a new successful sensitive and rapid detection for *Oxytetracycline* (*OTC*) and *Erythromycin* (*ERY*) antibiotics with detection limits of 2.714 nM and 3.306 nM, respectively. The proposed strategy provides an efficient detection way of tracing heavy metals *Hg*, *Cd*, and *Pb* with a detection limit of less than 5 ppm. Characterization of nanoprobe was by *UV/VIS* spectroscopy, X-ray Diffraction (*XRD*), Fourier-transform infrared spectroscopy (*FTIR*), and Transmission electron microscopy (*TEM*). The compared results were with graphene quantum dots (*GQDs*), graphene oxide quantum dots (*GOQDs*), and green synthesized silver nanoparticles (*AgNPs*) which were made from new extracts of aquatic plants and seaweeds from *Edku* and *Marriott* Lake. This novel Fluorescence quenching-based technique is sensitive, selective, less time-consuming and does not need expensive preparations to replace the commonly used chromatographic detecting techniques.

Keywords Silver/graphene quantum dots · Nanoprobe · Nanosensors · Aquaculture · Antibiotics · Optical sensors

List of symbols

$Ag@GQDs$ Silver/graphene quantum dots
OTC Oxytetracycline

<i>ERY</i>	Erythromycin antibiotics
<i>XRD</i>	X- ray diffraction
<i>FTIR</i>	Fourier-transform infrared spectroscopy
<i>TEM</i>	Transmission electron microscopy
<i>GQDs</i>	Graphene quantum dots
<i>GOQDs</i>	Graphene oxide quantum dots
<i>FAO</i>	Food and agriculture organization
<i>LOD</i>	Limit of detection
<i>ppb</i>	Parts per billion
<i>AgNPs</i>	Silver nano particles
<i>SPR</i>	Surface Plasmon resonance
<i>LSPR</i>	Localized surface Plasmon resonance
$AgNO_3$	Silver nitrate
<i>PL</i>	Photoluminescence spectroscopy
<i>FCC</i>	Face-centered cubic structure
<i>JCPDS</i>	Joint Committee on Powder Diffraction Standards
<i>D</i>	The average crystallite size of the silver particles
λ	The wavelength of the X-rays used for diffraction

✉ Amira H. E. Moustafa
amira.mostafa@alexu.edu.eg

Mahmoud A. Mousa
m.moussa@fsc.bu.edu.eg

Hanaa H. Abdelrahman
hana.hamam@alexu.edu.eg

Mamdouh A. Fahmy
ma.fahmy@niof.sci.eg

Dina G. Ebrahim
Sci.DinaGaber@alexu.edu.eg

¹ Faculty of Science, Alexandria University, Alexandria, Egypt

² Faculty of Science, Benha University, Banha, Egypt

³ Marine Chemistry Department, Environmental Division, National Institute of Oceanography and Fisheries (NIOF), Alexandria, Egypt

β	Full width at half maximum (<i>FWHM</i>) of a peak
I_0	The intensity, or rate of fluorescence, without the antibiotic
I	The intensity, or rate of fluorescence, in the presence of the antibiotic
K_q	The quencher rate coefficient
T_0	The lifetime of the emissive excited state without a quencher present
Q	The concentration of the antibiotic
K_{sv}	Stern–Volmer constant
T	The rate of fluorescence decay
DPV	Differential pulse voltammetry
AdSV	Amperometry and adsorptive stripping voltammetry
AdSDPV	Adsorptive stripping differential pulse voltammetry
CV	Cyclic voltammetry
SWV	Square wave voltammetry

Introduction

Increased food and drug administration demand results from the world population's continued growth. Furthermore, industrialization and urbanization are inevitable, accompanied by environmental pollutants (Mehwish et al. 2021). Nowadays, nanostructured materials have unique properties that make them ideal candidates for developing more advanced applications as biosensors and chemical sensors for detecting environmental contaminants such as heavy metal ions, phenolic chemicals, and poly-aromatic hydrocarbons, pesticides, and antibiotics (Naresh et al. 2021). In the present work, we focused only on aquaculture pollution. Fishes and other aquatic creatures are significant animal protein providers and other essential elements in people's diets. Marine animals and plants account for 17% of animal protein fed globally, over 40% of the world's population (Couture et al. 2021). According to Food and agriculture organization (FAO) estimations, aquaculture is one of the world's fastest-growing food-producing areas (FAO 2020; Shao et al. 2021). The excessive use of antibiotics in aquaculture increases rapidly. About 63,000 tons of antibiotics were used in 2010, which is expected to be 107,000 tons in 2030 (Tiseo et al. 2020). Introducing this high quantity of antibiotics into aquatic ecosystems may cause increase in the possibility of antibiotic-resistant bacteria, which produces an excellent problem for our life. Over 700,000 people die each year from illnesses caused by antibiotic-resistant bacteria. This number may rise to 10 million if left uncontrolled by 2050 (Heinrich et al. 2021).

Conversely, the pollution of aquaculture by heavy metals is a global issue. This pollution can be done by industrial

or home items, pesticides, and fertilizers containing heavy metals (Briffa et al. 2020). The contamination with heavy metals of Hg^{+2} , As^{+3} , Pb^{+2} , Cd^{+2} , and Cu^{+2} severely threatens human health and the environment. Because of their hazardous effects on plants, animals, and humans, they are non-biodegradable and accumulate in the food chain even at low concentrations. Presently, chromatographic and spectroscopic techniques can determine the metal ion levels in the water. However, they are expensive and need extensive technical training due to their complexity. Newly, nanosensors provide a new generation of determination of heavy metals with a limit of detection (*LOD*) up to 0.01 parts per billion (ppb).

Since the nanosize item reveals different properties of its bulk materials due to variations in its surface-volume ratio, the study and application of silver nanoparticles (*AgNPs*) have increased daily in recent years. They are easily produced from moderately stable silver (I) salts using various reducing agents (Mustapha et al. 2022). Optical, electrical, and thermal capabilities, as well as strong electrical conductivity and biological qualities, are all properties of *AgNPs* (Kumar et al. 2022).

Silver nanoparticles (*AgNPs*) are intriguing nanomaterials in colorimetric sensors, antimicrobial materials, chemical catalysis, and electrochemical sensor aspects (Seku et al. 2022). Recently, *Ag NPs* have been widely used for variable applications because of their distinctive surface Plasmon resonance (*SPR*) (Liu et al. 2021). The interaction occurring between the electrons on the surface of *Ag NPs* with electromagnetic radiation is called localized surface Plasmon resonance (*LSPR*). This type of interaction generates strong excitation and scattering spectra, around 400 nm in the visible range of the spectrum, so materials based on silver nanoparticles are suitable as optical sensors for detecting antibiotics and pesticides and are considered colorimetric sensors for heavy metals. Different methods can synthesize metal *NPs* such as *Ag NPs*; most use harmful chemical substances (AlMasoud et al. 2021).

In recent years, researchers have focused on the green synthesis of *Ag NPs*, which minimize the use of chemical agents, making nanoparticles more environmentally friendly, non-toxic, and cost-effective. Moreover, diverse substances may be used as reducing agents and stabilizers to synthesize *Ag NPs*. Carbon-based nanomaterials, especially quantum dots (*QDs*), have recently attracted significant attention as one of these materials.

Graphene quantum dots (*GQDs*) are nano-sized fluorescent carbon compounds with one dimension smaller than 10 nm. They can gain much attention as sensors or probes because of their low toxicity, low cost, good stability, high fluorescent activity (Sharma et al. 2021) and extensive surface modification. *GQDs* play an essential role not as reducing agents and preventing aggregation and oxidation of *Ag*

NPs only but also have an antibacterial properties of their own.

The present report will focus on the novel biosynthesis of *Ag NPs* by various rare aquatic plants and seaweed extracts from Edku and Marriott Lake Edku and Marriott Lakes, two of the five wetland lakes in Egypt's Northern Mediterranean basin. These *Ag NPs* can be used as a precursor for *Ag@GQDs* nanocomposite synthesis. Herein, we use fluorescent *GQDs* as stabilizers and reducing agents for producing *Ag@GQDs* nanocomposite with smaller particle sizes ranging from 2 to 9 nm. Advanced novel dual-function optical sensors promising from *Ag@GQDs* nanocomposite are studied. We demonstrate new effective analytical biosensor-based nanomaterials that successfully identify, measure, and confirm the presence of antibiotic residue to ensure that they are found in the authorized percentage.

Moreover, it demonstrate their ability as chemical sensors to detect heavy metal ions in aqueous solutions. It is essential to mention that this novel strategy does not recognize one type of antibiotic. Still, it identifies more than one type and determines the different concentrations of each, and others do not achieve this. We explain the unprecedented sensing strategy of the fluorescence nanocomposite *Ag@GQDs* to dispense with the standard time-consuming and expensive techniques. Moreover, to invent advanced environmentally friendly sensors for different future fields, this study will be concentrated on the possibility of applying the successful nanoprobe to aquaculture.

Experimental

Chemicals and materials

All chemicals were marked as reagent grade and used as received without further purification. Silver nitrate, extra pure ($AgNO_3$, 99.5%); citric acid monohydrate, $Cr(NO_3)_3 \cdot 6H_2O$, $Cu(NO_3)_2 \cdot 3H_2O$, $Hg(NO_3)_2 \cdot H_2O$, $Cd(NO_3)_2 \cdot 4H_2O$, $Pb(NO_3)_2$, KNO_3 , $Co(NO_3)_2 \cdot 6H_2O$ all were purchased from (Sigma-Aldrich) and (Merck Chemical Company). Nitric acid (HNO_3 , 72%) and sodium hydroxide ($NaOH$, 99%) pellets are extra pure from Oxford Lab Fine Chem. India, *Erythromycin*, Floroquin, and Penicillin were obtained from (Medical professions for veterinary products Co. *MUVCO*). Oxytetracycline hydrochloride was purchased from (Pharma SWEDEN). The tested antibiotics were prepared by calculating the equivalent active materials and weighing the respective powder.

Preparation of seaweeds and aquatic plant extracts from Edku & Marriott lakes

The seaweed samples were kept in a polyethylene bag with natural seawater to maintain the seaweed samples fresh. Preparation of aquatic plant extracts firstly by washing the collecting plants with tap water to remove both epiphytes and necrotic plants and then, distilled water to remove any associated debris. The plant samples were dried in an oven at 60 °C or shading at room temperature for two weeks, and the dried plants' materials were crushed as powder. 1 g of plant powder was weighed and mixed with double distilled water in a clean conical flask at room temperature for about 24 h and then, heated at 60 °C with stirring by a magnetic stirrer for 15 min. The extract was filtered using Whitman filter paper and stored filtrate in the refrigerator at 4 °C to keep them longer.

Green synthesis of *Ag NPs* by plant extracts from Lake of Edku & Marriott

By adding 10 ml of the filtrate (plant extract) to 90 ml of silver nitrate solution (1 mM) in a clean conical flask, the magnetic stirrer then stirred it at room temperature and *pH* 7.2 until the color changed from yellow to dark brown. This change indicates that the silver nitrate ($AgNO_3$) was reduced to *Ag* nanoparticles (*Ag NPs*) by alkaloids, flavonoids, and phenolic compounds, which could reduce and stabilize agents. Depending on the type, this change may occur immediately or after hours or days. Finally, centrifuged the obtained colloidal *Ag NPs* at 10,000 rpm and the supernatant was discarded. *Ag NPs* were washed with distilled water several times for further purification for characterization and applications.

Synthesis of graphene quantum dots (GQDs) & graphene oxide quantum dots (GO_{QDs}).

A typical process of *GQDs* is using 4 gm of citric acid in a 10 ml beaker and heating it to 200 °C in a furnace for 5 min. After 5 min, citric acid was liquefied, and the formation of *GQD* changed the color of the liquid from colorless to pale yellow, and after 30 min, it changed to orange. By continuous heating for 2 h, the orange color was converted to a black solid due to the formation of GO_{QDs} . The obtained orange liquid for preparing *GQDs* (2 gm) was added drop by drop into 200 mL of *NaOH* solution (0.2 M) under vigorous stirring by a magnetic stirrer. After neutralizing to *pH* 7.0 with *NaOH*, the aqueous solution of *GQDs* was stable and ready for characterization, and for the synthesis of *Ag@GQDs* nanocomposite, Acetic acid or Nitric acid can be used to adjust *pH* 7.0. The black solid (1 gm) was dissolved with

100 mL of NaOH (0.2 M) solution; the aqueous solution of GO_{QDs} was then neutralized.

Synthesis of AgNPs /GQDs nanocomposite

Ag@GQDs nanocomposite can be synthesized by mixing silver nanoparticles (previously prepared by green method from aquatic plants of *Edku & Marriott lakes*) with GQDs by volume ratio of 2:3, respectively, under ultra-sonication for 30 min; then, the mixture was centrifuged and dried.

Ag@GQDs nanocomposite can be prepared using GQDs as reducing and stabilizing agents. 10 ml of the previously prepared GQDs was diluted by 80 ml of double-distilled water. Then, pH was adjusted from 7 to 11 with the stock solution of NaOH (0.2 M). 1 ml of silver nitrate aqueous solution (0.1 M) was added to GQDs in a clean 250 ml beaker, and then, the mixture was heated to 85 °C under vigorous stirring by a magnetic stirrer for 2 h. The solution of black color converted to transparent, and Ag@GQDs nanocomposite precipitated. Finally, the solution was cooled at room temperature, and the product obtained was purified by centrifugation at 10,000 rpm and washing with deionized water several times (This method has been performed and characterized for applications as Nanoprobe).

Fluorescence measurements

First, prepare a stock solution of varying concentrations of antibiotics (*Oxytetracycline hydrochloride*, *penicillin*, *Erythromycin*, and *Floroquin*). We have prepared *Erythromycin* powder (Each 100 gm containing 20 gm of *Erythromycin* thiocyanate, MUVCO, Ismailia, ARE) by dissolving 0.2 gm at 1 L deionized water to prepare a stock solution of 0.04 gm/L from the active material. For *Oxytetracycline* hydrochloride powder (Each 1 gm contains 200 mg of tetracycline hydrochloride, SWEDE Pharma, ARE), we prepared it by mixing 0.2 gm with 1 L deionized water to produce 0.04 gm/L from the active material. But for *Floroquin* solution (10%, *FloroMed*, each 100 ml contains 10 gm of the raw material), the preparation has been done by mixing 0.4 ml with 1L deionized water to obtain 0.04 gm/L from the active material. On the other hand, *Penicillin* (United Co. for CHEM & Med (ACCMA), ARE) was mixed with deionized water. As we see, the concentrations of the active material of all antibiotics are constant to get accurate results. All these solutions were diluted to form the concentration series 0.04, 0.02, 0.01, 0.005, 0.00125 gm/L. Similarity stock solution of series metals ion $\text{Cr}(\text{NO}_3)_3 \cdot 6\text{H}_2\text{O}$, $\text{Cu}(\text{NO}_3)_2 \cdot 3\text{H}_2\text{O}$, $\text{Hg}(\text{NO}_3)_2 \cdot \text{H}_2\text{O}$, $\text{Cd}(\text{NO}_3)_2 \cdot 4\text{H}_2\text{O}$, $\text{Pb}(\text{NO}_3)_2$, KNO_3 , $\text{Co}(\text{NO}_3)_2 \cdot 6\text{H}_2\text{O}$ was prepared with different concentrations of 5, 10, 15, 30, 60, 125 and 500 ppm.

About 0.1 mL of a particular concentration of the antibiotic solution was added to 0.1 mL of Ag@GQDs nanocomposite solution and gently mixed for 5 min at room temperature. The solution was then ready for PL (Photoluminescence Spectroscopy) measurements using *PerkinElmer, model LS55 fluorescence Spectrophotometer*) at an excitation wavelength of 330 nm. The same technique was also repeated for the determination of the heavy metals.

Characterization (instruments)

X-ray diffraction (XRD) patterns were recorded on an X-ray diffraction spectrophotometer to investigate the crystalline structures of the synthesized materials using $\text{Cu K}\alpha$ radiation ($\lambda = 1.5406 \text{ \AA}$, operating voltage 45 kV, and current 40 mA) at a step size of 0.02° and 2θ range of $20\text{--}90^\circ$.

The morphology of the nanoparticles was characterized by a (TEM) transmission electron microscope (*JEM-1400 Plus, Japan*). The nanoparticle size was calculated using the image obtained. The sample was prepared as follows: nanoparticles were dissolved in distilled water, then sonication for 30 min for complete dispersion, then a single drop of nanoparticle solution was put onto the carbon-coated copper grid (400 mesh) and dried at room temperature.

FTIR spectra were recorded using (*Nicolet 6700, Nicolet, United States*). All spectra were determined in a range of $4000\text{--}400 \text{ cm}^{-1}$ using pellets obtained by mixing *KBr* (*Sigma-Aldrich*) with purified powder of the prepared nanoparticles.

UV–vis absorption spectrum was analyzed using (*Thermal Scientific, model: EVO300*).

Results and discussions

Transmission electron microscope (TEM) analysis

TEM was used to clarify the prepared nanomaterials' morphologies and particle size. TEM was performed for the green synthesized nanosilver from plants of *Edku and Marriott*. The TEM images are illustrated in Table 1, which shows that the nanoparticles were primarily spherical, with an average size of 14–30 nm. TEM images of GQDs, graphene oxide quantum dots and Ag@GQDs nanocomposite are illustrated in Fig. 1. As illustrated in Fig. 1a, b, TEM images for GQDs and graphene oxide show dots with a diameter size distribution range between 1.5 and 4 nm. Figure 1c shows a high-resolution picture of graphene quantum dots. For Ag@GQDs, nanocomposites are illustrated in Fig. 1d. GQDs were combined with Ag NPs to get particles with an average diameter of 1–9 nm.

Table 1 Edku & Marriott plants samples that were used and treated for Ag NPs synthesis


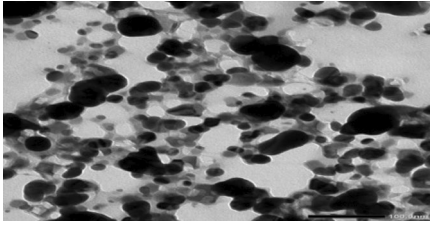

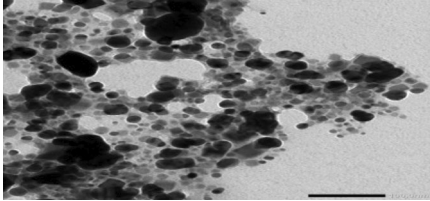

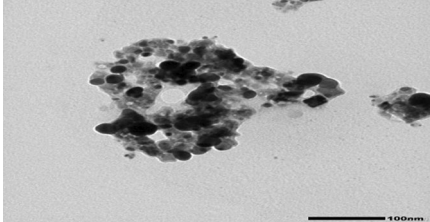

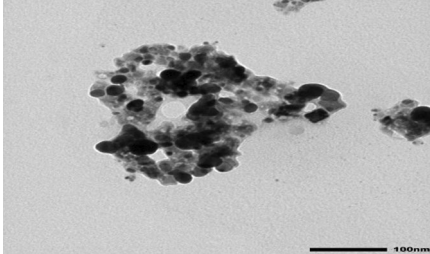

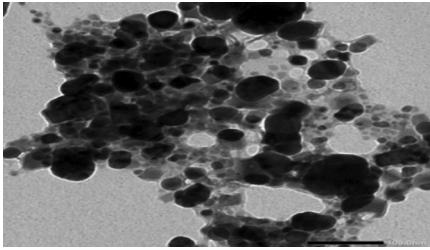

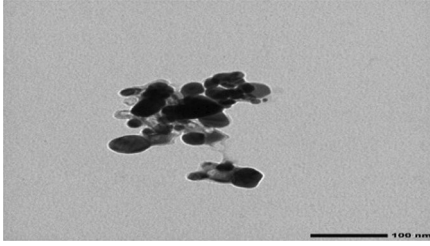

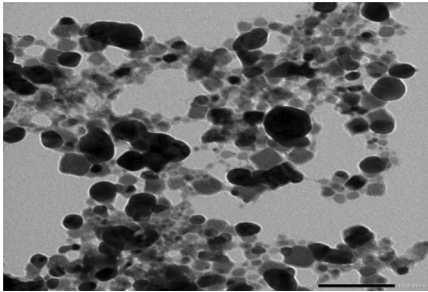

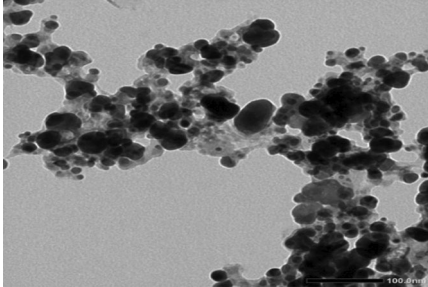
Species name	Image	Average size	TEM
1. <i>Eichhornia crassipes</i>		23 nm	
2. <i>Pistia Stratiotes</i> (Water cabbage) (Water Lettuce)		17 nm	
3. <i>Typha Capensis</i>		15 nm	
4. <i>Scirpus Maritimus</i>		18 nm	
5. <i>Najas Marina</i> (Spiny water nymph) (spiny naiad) (holly-leaved naiad)		26 nm	
6. <i>Potamogeton Pectinatus</i>		27 nm	

Table 1 (continued)

Species name	Image	Average size	TEM
7. <i>Ludwigia Stolonifera</i>		14 nm	
8. <i>Schoenoplectus validus</i>		23 nm	

FTIR analysis

FTIR enables the in situ analysis to identify and confirm nanoparticle formation and investigates the surface adsorption of functional groups on nanoparticles. FTIR analysis was performed for the synthesized nanoparticles and nanocomposites at the wavenumber region of 500–4000 cm^{-1} . The results are illustrated in Fig. 2. The band observed at a wavenumber of 445–470 cm^{-1} indicates the presence of silver (Ag). Also, we detected the axial stretching frequency of (–N–H) at 3277 cm^{-1} , the (–C–H–) group at 2917 cm^{-1} , carbonyl (–C=O) stretching vibration at 1613 cm^{-1} , and the (–C–O) at 1051 cm^{-1} indicating the presence of functional groups (alkaloids, flavonoids, and phenolic compounds) which work as reducing and stabilizing agents. Furthermore, the polyphenol compounds also reduce Ag^+ to Ag NPs. The groups corresponding to aromatic structures and the band of polyphenols were observed at 1516 cm^{-1} and 1320 cm^{-1} , respectively. The characteristic bands in FTIR spectra of GQDs and GO at wavenumbers 1384, 1658, and 1642 cm^{-1} correspond to –COO, C–O, and C=C, respectively. These bands indicate the occurrence of complete carbonization of the citric acid. The CH stretching peak of C(=O)–H is observed at 2553 cm^{-1} . The stretching vibration in the FTIR spectrum of GQD (C–O–C) cannot be detected, so there is no characteristic feature of graphene oxide (GO). However, a strong vibration band is

observed at 3450–3508 cm^{-1} , indicating the presence of the OH stretching group. It is explained how the chemical groups in GQDs change when Ag NPs are added; the broad absorption band at 625 cm^{-1} is enhanced in the presence of Ag–O. The development of a hydrogen bond caused by the combination of GQDs and Ag nanoparticles made the stretching vibration of the O–H strong. Stretching vibrations of –COOH peaked between 1613 and 1652 cm^{-1} of Ag@GQDs' COOH was higher than that of GQDs (Zhang et al. 2020). C–O–C was positioned at 1123 cm^{-1} ; however, as Ag@GQDs formed, their absorption peaks became sharper. The obtained FTIR spectra were in perfect agreement with previous investigations; it confirmed the synthesized nanomaterials were GQDs/Ag nanocomposites (Mandal et al. 2019).

x-ray diffraction (XRD)

To investigate the crystalline structures of the synthesized silver nanomaterial, XRD patterns were used. XRD of GQDs and GO_{QDs} represented in Fig. 3a, b shows an amorphous diffraction peak at an angle $2\theta = 23^\circ$ corresponding to (002) plane of SP^2 hybridization of graphene structure referring to the formation of highly disordered carbon atoms of GQDs (Sharma et al 2017). A characteristic diffraction peak at an angle $2\theta = 10^\circ$ corresponds to the (001) plane for GO_{QDs} , as reported by ((Perera et al. 2018) ACS Nano.2010;4:4806 Fig. 3c revealed peaks at (2θ) of 38.17°, 44.37°, 64.5°, 77.5°

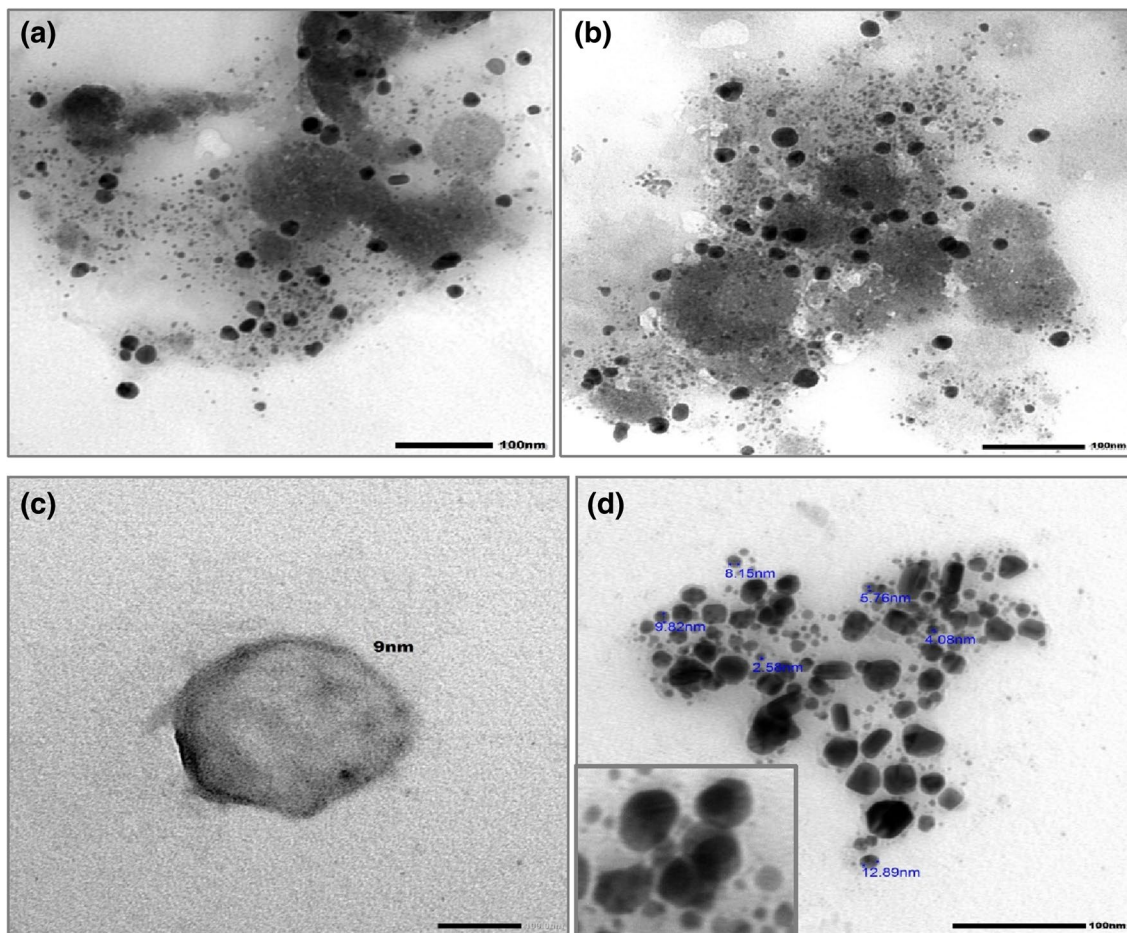


Fig. 1 TEM images of **a** GQDs, **b** graphene oxide quantum dots (GO_{QDs}), **c** high resolution and magnification pictures of GQDs, **d** Ag/GQDs nanocomposites

and 81.69° characterized for (111), (200), (220), (311), and (222) planes, respectively, of the cubic crystalline face-centered cubic structure (FCC) of silver, then compared with the standard powder diffraction card of JCPDS (Joint Committee on Powder Diffraction Standards), silver file No. 04–0783. The average crystallite size D of the silver particles has been estimated by using the Debye–Scherer's Formula, $D = 0.9\lambda/\beta \cos\theta$, where λ is the wavelength of the X-rays used for diffraction and β is full width at half maximum (FWHM) of a peak (Rajeev et al. 2022). XRD pattern indicates that the synthesized Ag NPs were composed of pure silver with no presence of silver oxide. The broadening of the Bragg's peak indicates the formation of nanoparticles. It was found that the calculated average crystallite size from XRD is quite close to the assumed from TEM. The result of the average particle size of AgNps was calculated using the Scherrer formula from XRD, which is represented in Table 2. Furthermore, the XRD pattern of Ag@GQDs is represented in Fig. 3d. Ag@GQDs composite also shows an amorphous structure from the presence of GQDs and

characteristic diffraction peaks of the silver nanoparticles crystal structure appeared (Quyen et al. 2021) As a result, it is proven that Ag@GQDs nanocomposite was completely formed as predicted.]

UV–Vis spectroscopy

The UV–visible spectra of the investigated samples are represented in Fig. 4a. As illustrated, for two different plants, *Scripus Maritimus* and *Najas Marina*, a characteristic absorption band of about 380 and 410 nm, respectively, is observed due to the surface Plasmon absorption of Ag NPs (FuL et al. 2021). It is important to mention that all the investigated plants as the same absorption band. The UV–Vis spectrum of GQDs and GO_{QDs} in an aqueous medium is represented in Fig. 4-b, c, respectively, and exhibits an absorption peak at 330 nm and 355 nm due to the absorption of the graphitic structure and the presence of $\pi-\pi^*$ transition of Sp^2 carbon (–C–C–) bonds (Bokare et al. 2020) Interestingly, a slightly red shift of UV–visible absorption spectra

Fig. 2 FTIR spectra of **a** *GQD*, **b** graphene oxide quantum dots (*GO_{QDs}*), **c** *Ag NPs*, **d** *Ag/GQDs* nanocomposites

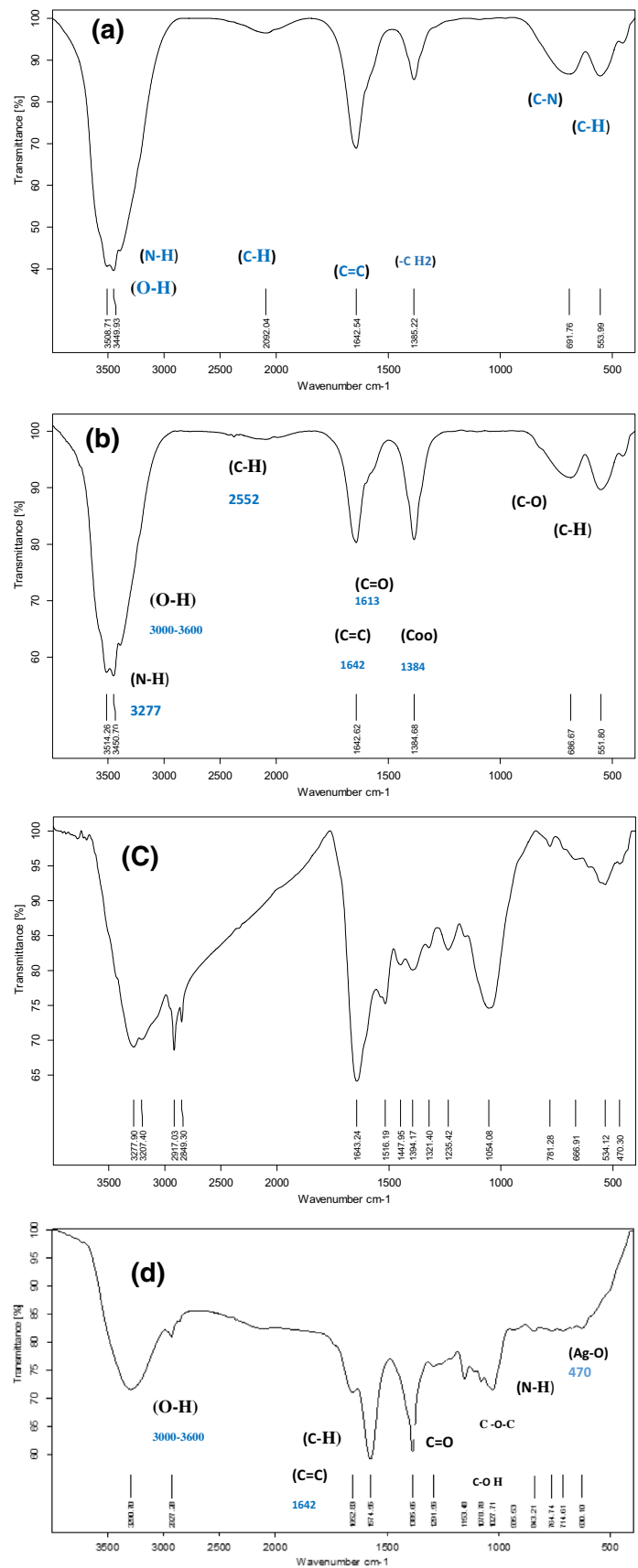


Fig. 3 XRD pattern of **a** *GQD*, **b** graphene oxide quantum dots (*GO_{QDs}*), **c** *Ag NPs*, **d** *Ag/GQDs* nanocomposites

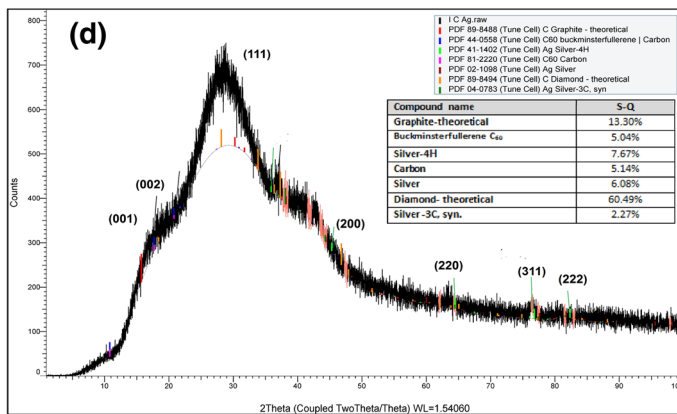
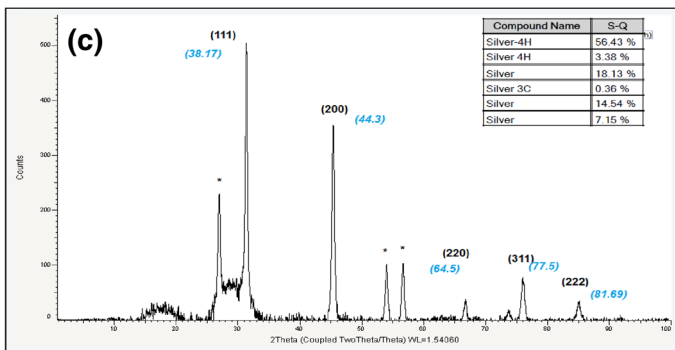
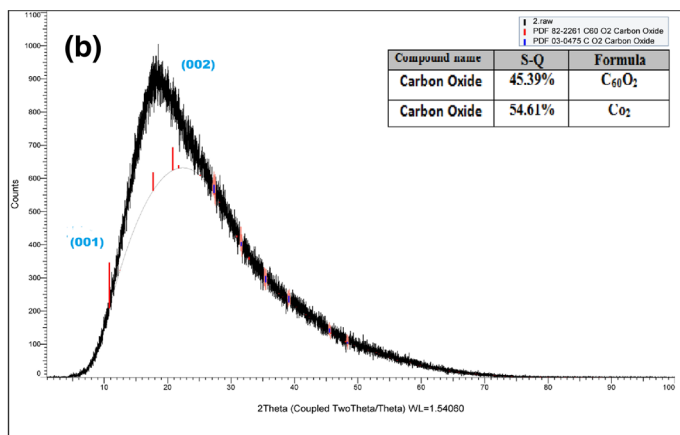
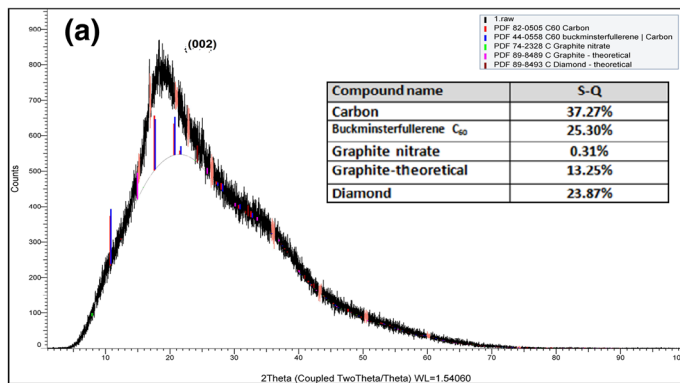


Table 2 The average particle size of silver nanoparticles calculated using the Scherrer formula from XRD

$X(2\theta)$	θ	$\text{Cos } \theta$	$Y(\text{counts})$	dY	Time	$D(\text{nm})$	Average particle size
38.173	19.086	0.972177	240	15.5	19.2	23.55	17.1 nm
44.370	22.185	0.98126	230	15.2	19.2	20.39	
64.5	32.25	0.6718	81.0	9.0	19.2	14.4	
77.5	38.75	0.4968	41.0	6.40	19.2	12.3	
81.691	40.84	-0.999	40.0	6.32	19.2	11.7	

and change in the color of the solution (the brown color became darker) was recorded due to the alkaline medium of *NaOH* and high *pH* during preparations. The *Ag@GQDs* nanocomposites are illustrated in Fig. 4d as shown by the typical absorption peaks of both *GQD* at 330 nm and *Ag NPs* at 400 nm, which attributed to *LSPR* of silver nanoparticles with slight shifts in their positions due to their interaction and that demonstrates that silver completely combines with *GQDs* to create *Ag@GQDs* nanocomposites. The *UV* spectrum of nanocomposite was another proof of *Ag@GQDs* nanocomposite production.

Photoluminescence spectroscopy (PL)

Photoluminescence spectroscopy (*PL*) is an efficient technique to examine the crystal quality and the presence of impurities in crystals. It is possible to interpret the photoluminescence of noble metals as the excitation of electrons from occupied d-band states into states above the fermi level. Following electron–phonon and hole–phonon scattering, energy is lost, and then, an electron from a *sp* band recombines with a hole to produce a photoluminescent reaction (Vinay et al. 2019).

Photoluminescence (*PL*) spectra of the green synthesized *Ag NPs* are shown in Fig. 5. A fluorescence study was investigated to evaluate the optical properties of the *Ag NPs* in an aqueous medium. The exciting wavelength was 200 nm. The peaks observed at 430 nm were attributed to the relaxation of the electronic motion of surface Plasmon; the intensity change from one plant to another may be attributed to the component of the plant and the capping agents coating the nanoparticles.

Two emission bands at 430 nm and 480 nm compensate for the spectra. The *PL* peak at 430 nm can be attributed to the radiative recombination of electrons and holes from the *sp* conduction band. But the emission at 480 nm represents the *SPR* of *AgNPs* (Varghese et al. 2020) (Kamakshi et al. 2018).

The emission at 530 nm is so faint that it can be overlooked in the whole photoluminescence spectrum. It may attribute to the presence of phytochemical component impurities.

According to *XRD* and *TEM* findings, the average size of *Ag NPs* and *Ag@GQDs* was between 2 and 25 nm. With

this dipole limit, it is thought that nanoparticles whose diameter is significantly smaller than the wavelength of light will respond as a dipole in an optical field. As a result, their absorption and emission should be predominantly coherent with their surface excited energy band or active surface sites. This was previously reported (Zhang et al. 2008). Previous researchers have discovered that strong emission bands may be attributed to *Ag–Ag* interactions.

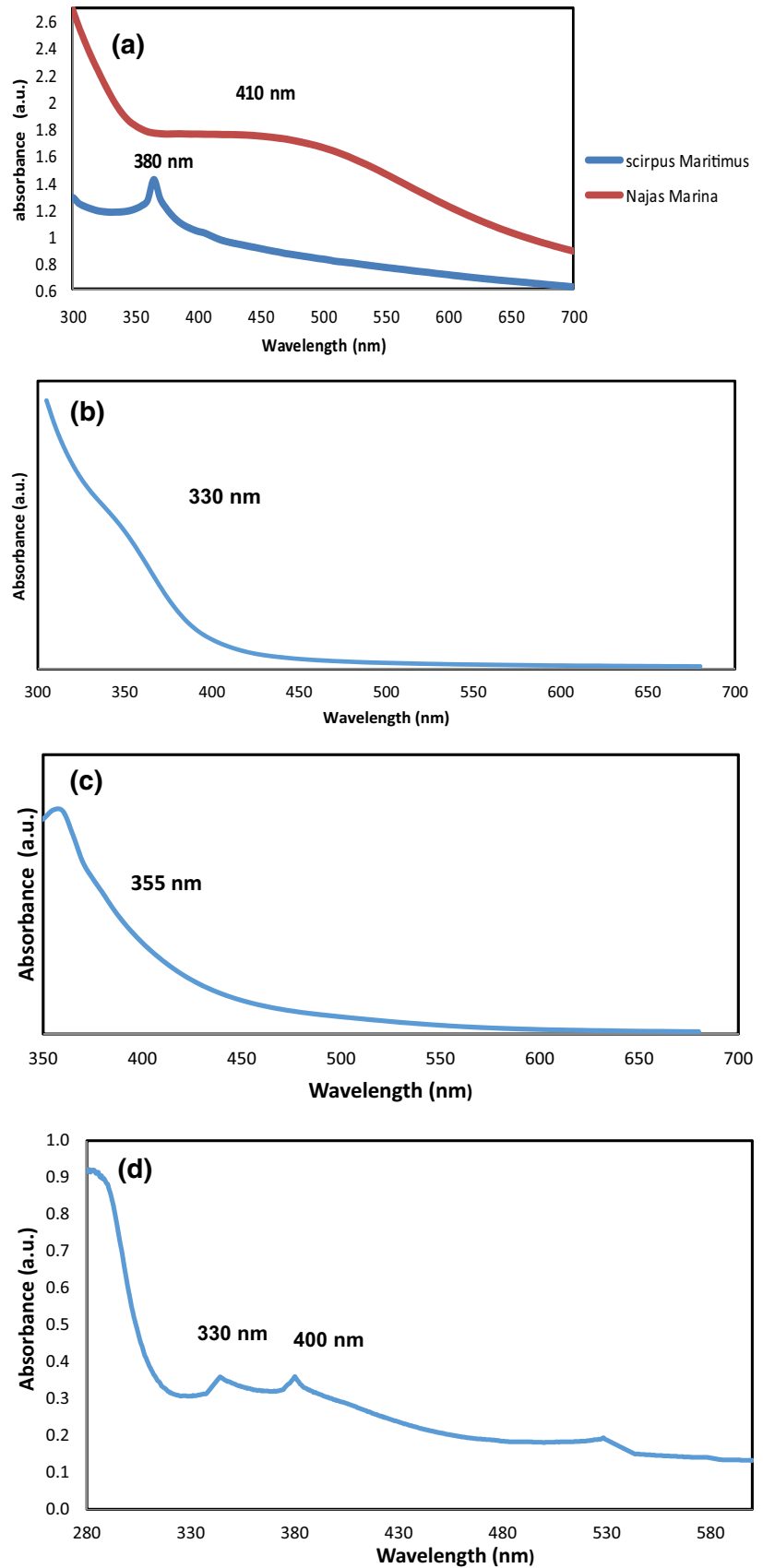
The optical properties of the synthesized *GQDs* and *GO_{QDs}* were also studied using *PL* spectroscopy. The fluorescence spectra of *GQDs* and *GO_{QDs}* at different exciting wavelengths are demonstrated in Fig. 6a and b, respectively. Figure 6a illustrates *GQDs* fluorescence peaks at different excitation wavelengths 350, 300, and 280 nm; the *PL* fluorescence peaks were observed at the same wavelength, 500 nm, without any shift. It is observed that fluorescence intensity decreases when the excitation wavelength moves from 280 to 350 nm. However, Fig. 6b shows the fluorescence of the *GO_{QDs}* at 580 nm using different excitation wavelengths of 400 and 350 nm.

A comparison of fluorescence spectra between *GQDs* & *GO_{QDs}* excited at 350 nm is demonstrated in Fig. 6c. It was found that the intensity of *GQDs* was greater than that of *GO_{QDs}* at the same excitation wavelength of 350 nm. So it is crucial to mention that it is possible to benefit from *GQDs* in developing chemical sensors, as we will discuss in the research. Therefore, *GQDs* have been chosen in our work for doping with *Ag NPs* for more applications mentioned above.

The optical properties of *Ag@GQDs* were studied using *PL* spectrum data for different excitation wavelengths of 330, 340, 350, and 370 nm. The results are represented in Fig. 7a. The results show fluorescence peaks at around 430, 480, and 540 nm.

These peaks are attributed to the *LSPR* (localized surface plasmon resonance) absorption peak of *Ag* nanoparticles besides the surface defects of the graphitic structure, where the *GQDs* show fluorescence peak at 480 nm at excitation wavelength 330 nm, see Fig. 7b. The most important observation is that for the same excitation wavelength of 330 nm, the fluorescence peak of *Ag@GQDs* appears at a higher intensity than those observed for *Ag NPs* and *GQDs*. That makes the *Ag@GQDs* a promising material for many novel applications.

Fig. 4 Comparisons of UV–vis absorption spectra of **a** Ag NPs from two different plants *Najas Marina* and *Scirpus Maritimus* **b** GQDs, **c** GOQDs, and **d** Ag@GQDs composites



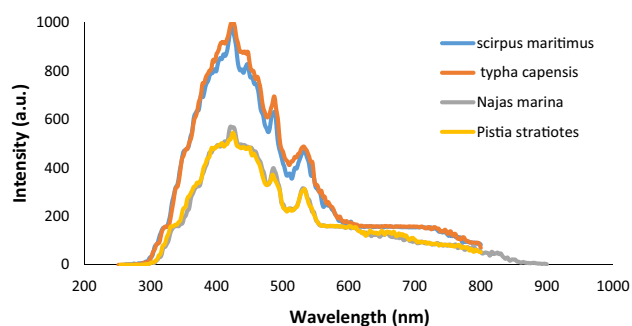


Fig. 5 PL spectra of Ag NPs were synthesized by different plants and seaweeds of Edku & Marriott Lake at excitation wavelength 200 nm

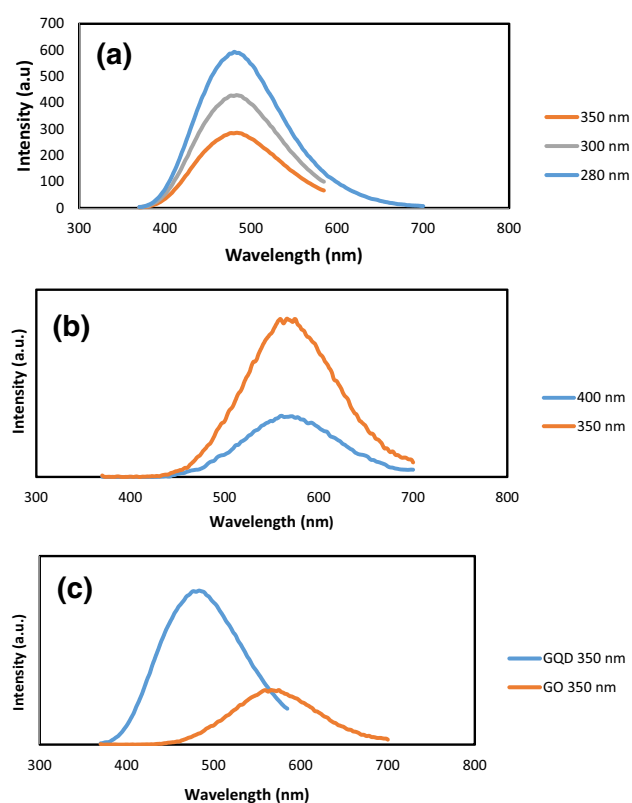


Fig. 6 **a** Photoluminescence spectra of *GOQDs* at different excitation wavelength 280,300 and 350 nm, **b** photoluminescence spectra of *GOQDs* at different excitation wavelength 350 and 400 nm **c** comparison of fluorescence spectra of *GQDs* & *GOQDs* excited at 350 nm

It is essential to mention that Fig. 7b shows a comparison of fluorescence spectra of *Ag@GQDs* nanocomposites to *GQDs*, which illustrates a significant increase in fluorescence. The adsorption of graphene on the Ag (111) surface results in weak bonding, which preserves the electronic structure (Kachel et al. 2020; Ho et al. 2021). The distance between the plasmonic nanoparticles and the fluorescence material can determine whether *PL* is enhanced or quenched (Badshah et al. 2020; Fernández et al. 2021). The mentioned

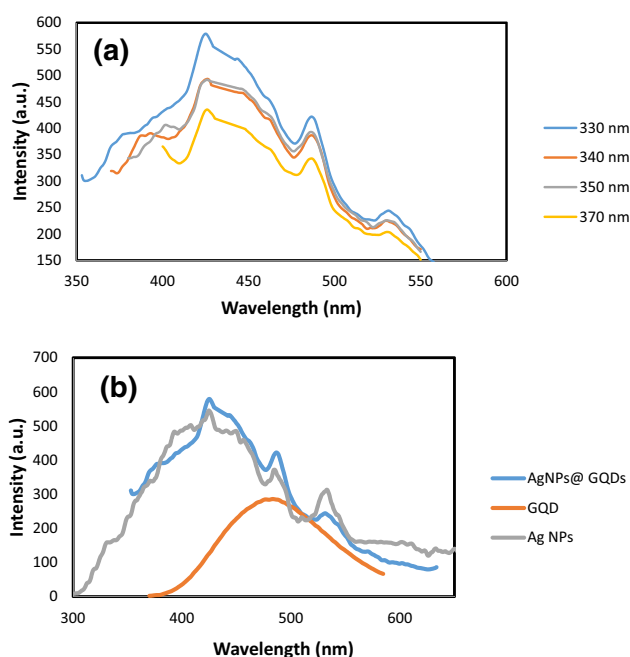


Fig. 7 **a** PL spectra of *Ag@GQDs* nanocomposites at different excitation wavelengths. **b** Comparison of fluorescence spectra of *GQDs*, *Ag NPs*, and *Ag@GQDs* nanocomposites excited at 330 nm

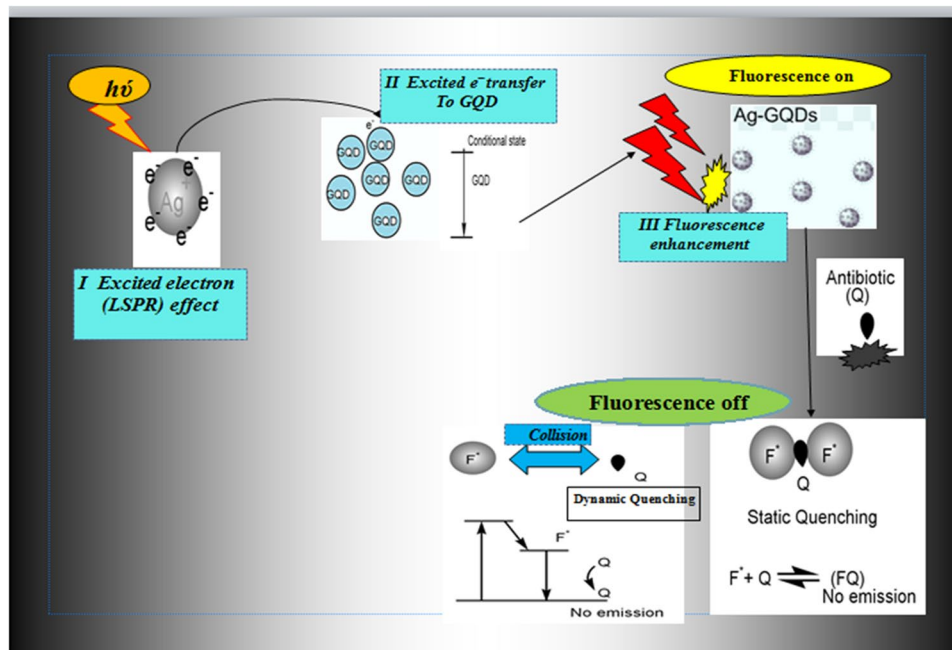
procedure (using *GQDs* as reducing and stabilizing agents.) did not introduce any extra stabilizer in the *Ag@GQDs* system, so the plasmonic nanoparticle *Ag* was directly associated with the fluorescent material *GQDs*. This association enhances the fluorescence because it can facilitate the ejection of *LSPR* (Localized Surface-Plasmon Resonance) excited electrons on *Ag* into the fluorescence material *GQDs* (Bokare et al. 2020). We can benefit from doping with silver nanoparticles in this work. When *Ag* and *GQDs* are combined, the electrons that may be localized on *AgNPs* can be transferred between the two sensing nanomaterials, resulting in sensing (Tang et al. 2019).

The process involves the following mechanism:

- Step (1): *LSPR* excited electrons would oscillate on the surface of the plasmonic nanoparticle *Ag NPs* under visible light.
- Step (2): With the increase in electron density, electron transfer from *Ag* to the conduction band of *GQDs*.
- Step (3): The electron returns to the ground state, so the vast amounts of hot electron transfer eventually lead to fluorescence enhancement. All these steps are explained in Fig. 8.

Doping agents or functionalized *GQDs* have been suggested to increase sensitivity and specificity. Using Ag^+ metal ions, the selectivity and functionality of *GQDs* have been assessed. Additionally, change in the optical

Fig. 8 Schematic illustration represent the mechanism of Ag/GQDs fluorescence enhancement, the role of the quencher (antibiotic OTC) and the difference between static and dynamic quenching



characteristics of GQDs, the synthesized Ag@GQDs nanocomposite offers a high surface area/volume ratio and active sites for the adsorption of antibiotic compounds. It can also change the band gap, causing a saturation effect or an increase in fluorescence, which might be used to create sensors (Buniyamin et al. 2022).

It is well known that the amount of aromatic rings in antibiotics affects the adsorption rate most significantly (Peng et al. 2016). Different aromatic rings found in antibiotics boost their ability to bind to the surface of Ag@GQDs. This indicates that the antibiotic will adsorb to carbon-based materials more quickly the more aromatic rings it has. As previously reported, π - π interaction is the main mode by which antibiotics bind to Ag@GQDs (Kauffman et al. 2010).

Based on these studies, we used the plasmonic particles as (Ag NPs) to improve the fluorescence of GQDs presents great benefits as LSPR-enhanced fluorescence to achieve high sensitivity for variable applications as probes:

(a) Ag@GQDs for detection of antibiotics

High concentration residue of antibiotics in aquaculture and water is a severe problem. The most commercially available antibiotics in Egyptian aquaculture are *Oxytetracycline hydrochloride*, *Erythromycin*, *Penicillin*, and *Floroquin*. Therefore, they were selected to study their luminescent sensing performances with Ag@GQDs nanocomposite as a chemo-sensor. The results demonstrated a fluorescence quenching response for *Oxytetracycline hydrochloride* and *Erythromycin* more than the other antibiotics but to different

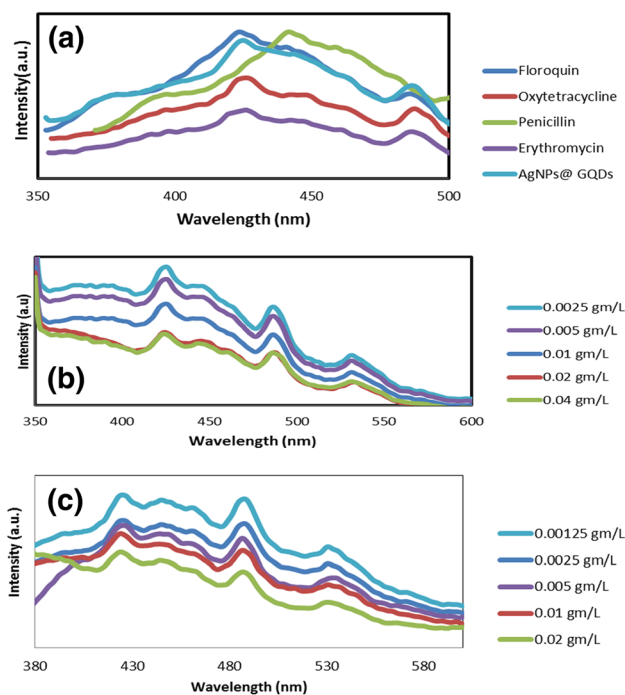


Fig. 9 a Representative fluorescence-quenching spectrum of Ag/GQDs upon adding variable antibiotics. b Concentration-dependent Fluorescence quenching of Ag/GQDs with addition Erythromycin. c Concentration-dependent Fluorescence quenching of Ag/GQDs with addition Oxytetracycline

degrees Fig. 9a. The results also showed that *Oxytetracycline hydrochloride* and *Erythromycin* exhibit a more significant fluorescence quenching effect. Figure 9b and c shows the

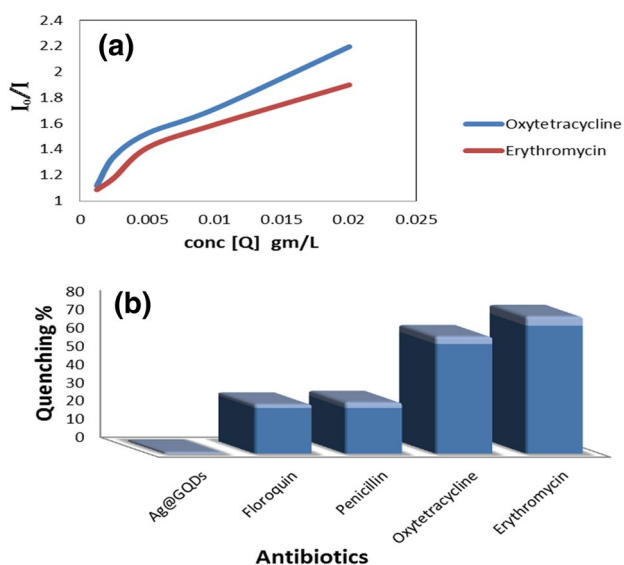


Fig. 10 **a** Stern–Volmer Fluorescence quenching plot of detecting antibiotics Oxytetracycline & Erythromycin. **b** Quenching percentage diagram to demonstrate antibiotics selective efficiency for the investigated Ag/GQDs composites signals

relationship between the concentration and fluorescence intensity for *Oxytetracycline* and *Erythromycin*, respectively. As the concentration increases, fluorescence quenching occurs.

Moreover, that demonstrates the unprecedented sensitivity and selectivity of Ag@GQDs nanocomposite. So it is considered a new successful sensing probe not for one type of antibiotic but can also differentiate between different classes. So *Oxytetracycline* and *Erythromycin* were selected to define their detection efficiency by the Ag@GQDs nanocomposite by determining the relationship between the antibiotics' concentrations and the composite's fluorescence intensity. The results in Fig. 10a showed that the fluorescence is inversely proportional to the antibiotics concentrations. That means the luminescence intensities steadily decrease, and the fluorescence quenching occurs with the antibiotic's continuous addition (concentration increase) according to the Stern–Volmer equation (Juneau et al. 2022):

$$I_0/I = 1 + K_q T_o [Q] \quad (1)$$

where I_0 is the intensity, or rate of fluorescence, without the antibiotic, I is the intensity, or rate of fluorescence, in the presence of the antibiotic, K_q is the quencher rate coefficient, T_o is the lifetime of the emissive excited state without a quencher present, and $[Q]$ is the concentration of the antibiotic. Higher I_0/I indicate that the probe has excellent sensitivity and selective detection of the antibiotic.

The selectivity test for the investigated Ag@GQDs nanocomposites for different antibiotics, especially

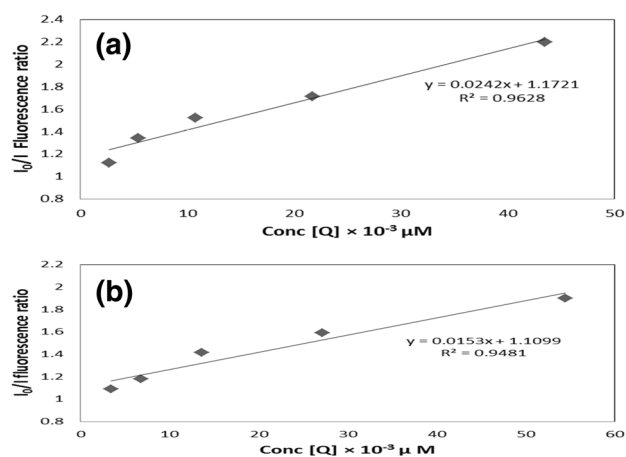


Fig. 11 Fluorescence intensity performance with variable antibiotics concentrations: **a** A Linear relationship between fluorescence ratio and concentration [Q] of Oxytetracycline. **b** Linear relationship between fluorescence ratio and concentration [Q] of Erythromycin

Oxytetracycline hydrochloride and *Erythromycin*, is shown in Fig. 10b. The fluorescence quenching percentages plot illustrates the sensitivity of the synthesized Ag@GQDs for the detection of antibiotics (*Oxytetracycline* & *Erythromycin*) more than any other antibiotics.

The quenching process can be classified as static or dynamic depending on the quenching mechanisms. It is represented in Fig. 8. The quencher and the fluorescence probe create a bound non-fluorescent complex during the static quenching process. It is known that the number of these complexes tends to increase with the increasing concentration of quencher molecules (Alexiev et al. 2014). But the corresponding fluorescence lifetime (fluorescence decay rate) is independent of the quencher concentrations $[Q]$ (Chini et al. 2019). Whereas in the case of dynamic quenching, the quencher molecule collides with the fluorophore in the excited state and is responsible for the variation in quencher concentrations. So that the change of K_{sv} and corresponding lifetime value T decrease with the increase in $[Q]$ quencher concentrations as the following equation:

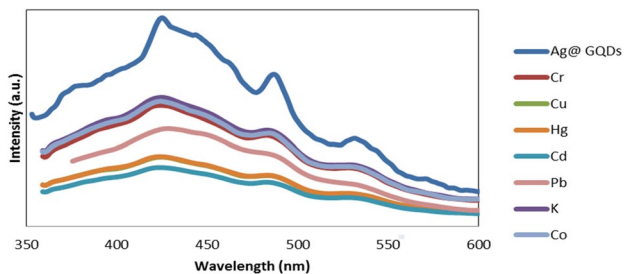
$$K_{sv} = K_q \cdot T \quad (2)$$

where K_{sv} is the Stern–Volmer constant, and T is the fluorescence decay rate. According to the Fluorescence, the plot represented in Fig. 11a, b, a good linear relationship between the fluorescence ratio I_0/I and the Concentration $[Q]$ of the antibiotics is obtained with a linear range of 2–50 μM for *Oxytetracycline* and 3–60 μM for *Erythromycin*. The corresponding regression coefficient R^2 for *Oxytetracycline* and *Erythromycin* are 0.9628 and 0.9481, respectively, confirming the linear relationship. The change in PL intensity of the prepared nanocomposite in the presence of antibiotics with

Table 3 Silver/graphene quantum dots were quenched by Oxytetracycline and Erythromycin

Antibiotics	Linear regression equations	Correlation coefficient R^2	Linear range	Limit of detection (LOD)
Oxytetracycline	$I_0/I=0.0242[Q]+1.1721$	0.9628	2.0–50 μM	2.0 nM
Erythromycin	$I_0/I=0.0153[Q]+1.1099$	0.9481	3.0–60 μM	3.3 nM

The detection limit is defined by the equation $\text{LOD}=3 \delta/K$, where δ is the standard deviation ($n=10$) and K is the slope of the calibration plot

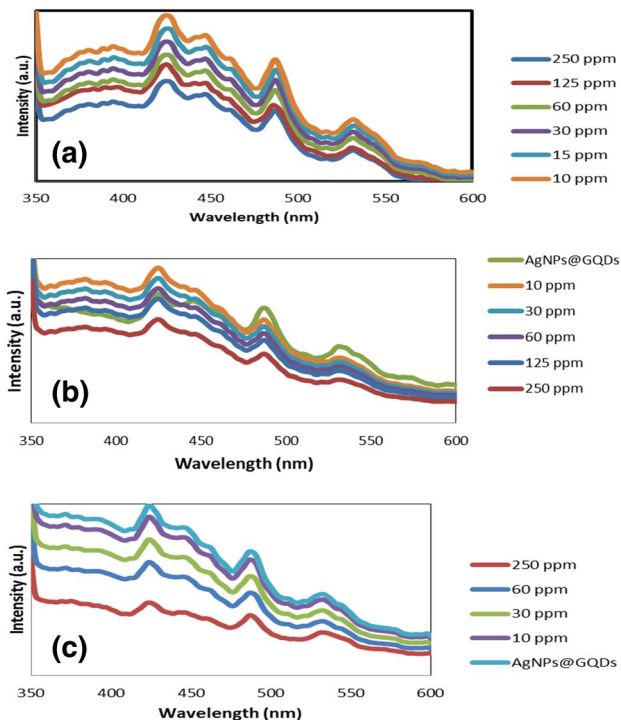
**Fig. 12** Representative Fluorescence quenching spectrum of Ag@GQDs upon adding variable heavy metals (conc. 10 ppm)

variable concentrations was observed. It is noticeable that the fluorescence was quenched gradually with the increased concentration of antibiotics. The complete data are discussed in Table 3.

(b) AgNPs/GQDs for detection of heavy toxic metals

Fluorescence experiments were designed to identify the heavy metals sensing capabilities of Ag@GQDs nanocomposite. The fluorescence intensities in the presence of heavy metals are lower than the fluorescence intensities of the free nanocomposite. That confirms the successful conjugation of the nanocomposite with the heavy metal ion to produce detectable signals. The data presented in Fig. 12 show that the Co^{2+} , K^+ , Cu^{2+} , and Cr^{3+} ions with nearly the same fluorescence quenching intensities are higher than those observed for Hg^{2+} , Pb^{2+} , and Cd^{2+} . This height means that the nanocomposite is more sensitive to Hg^{2+} , Pb^{2+} , and Cd^{2+} than the other investigated ions. So Ag@GQDs can provide a new successful Nanoprobe for precisely detecting specific heavy metals.

Results presented in Fig. 13 show that the photoluminescence intensity decreases with the increase in the concentrations of heavy metals ions Hg^{2+} , Pb^{2+} , and Cd^{2+} , so it is considered ions concentration dependence and that demonstrated in the three independent experiments, which are reflected in values corresponding to PL fluorescence intensities. With a high concentration of Hg^{2+} , Pb^{2+} , and Cd^{2+} , a significant quenching is observed in Fig. 13a–c, respectively. These show a high sensitivity of the novel fluorescent sensor

**Fig. 13** a Fluorescence spectra of Ag@GQDs with different Hg^{2+} concentrations. b Fluorescence spectra of Ag@GQDs with different Pb^{2+} concentrations. c Fluorescence spectra of Ag@GQDs with different Cd^{2+} concentrations

Ag@GQDs nanocomposite. The Ag@GQDs -based optical sensor is employed for detecting different heavy metals in an aqueous solution with detection limits less than 5 ppm with good sensitivity and selectivity for Hg^{2+} , Pb^{2+} , and Cd^{2+} ions recognition.

It is essential to mention that Ag@GQDs nanocomposite can detect several metal ions M^+ and M^{2+} , with smaller concentrations of less than 5 ppm via fluorescence quenching. The fluorescence quenching of Ag@GQDs nanocomposite is also sensitive to several antibiotics. This sensitivity means that the Ag@GQDs sample is an excellent, novel dual-function chemo-sensing material for antibiotics and heavy metals.

The selectivity test results for the researched Ag@GQDs nanocomposites for Hg^{2+} , Pb^{2+} , and Cd^{2+} are shown in Fig. 14. The fluorescence quenching percentages plot shows

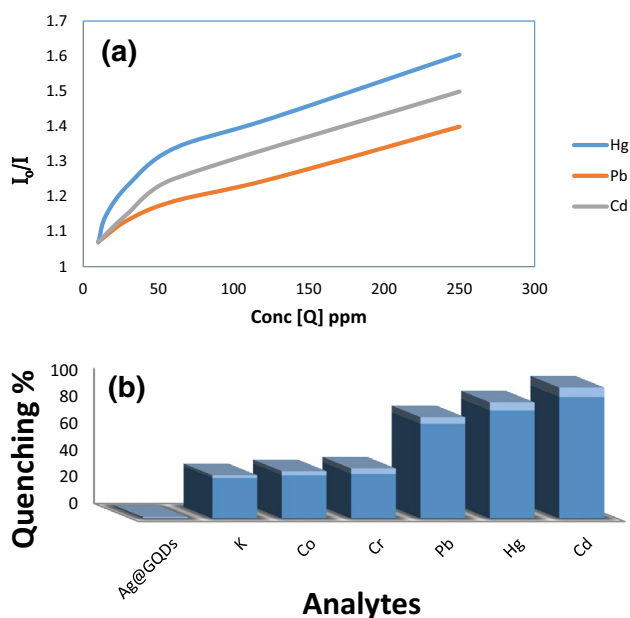


Fig. 14 **a** Stern–Volmer Fluorescence quenching plot for some toxic heavy metals *Hg*, *Pb*, and *Cd*. **b** Quenching percentage diagram to demonstrate the selective efficiency for the investigated *Ag@GQDs* composites signals

that the synthesized *Ag@GQDs* are sensitive to specific metals more than others. Quenching efficiency is studied and presented in Fig. 15 for the proposed fluorescence sensor to highlight variable future directions. The results explain the fluorescence intensity of *Ag@GQDs* nanocomposites in the absence and presence of the quencher (Hg^{2+} , Pb^{2+} , and Cd^{2+} ions). The fluorescence intensity decreases rapidly with increasing concentrations of metal ions. The sensitivity of fluorescence quenching can be effectively related to the Stern–Volmer constant (K_{SV}) using the following equation;

$$I_0/I = 1 + K_{SV}[Q] \quad (3)$$

where I_0 and I are the fluorescent intensities of solute molecules in the absence and presence of a quencher, respectively, and $[Q]$ is known as the analyte concentration (Sathathi et al. 2018). The higher K_{SV} value for these heavy metal analytes can be attributed to the efficient interaction of these heavy metal ions with the proposed sensor, which ultimately leads to a significant Fluorescence quenching. A robust linear relationship between the fluorescence ratio I_0/I and the concentration of the analyte $[Q]$ was illustrated with the linear range at 5–250 ppm for Hg^{2+} , according to the Fluorescence plot shown in Fig. 15. The correlation coefficients R^2 for Hg^{2+} , Pb^{2+} , and Cd^{2+} are 0.9043, 0.9768, and 0.9533, respectively, indicating that the linear association exists with a limit of 5 ppm. And the results are illustrated in Table 4.

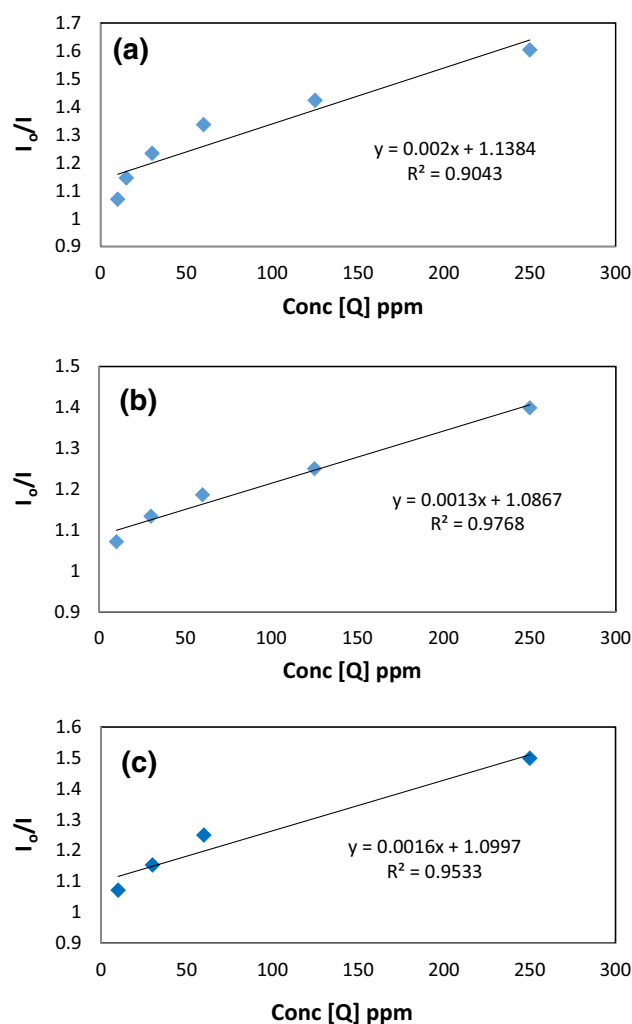


Fig. 15 Linear relationship between fluorescence ratio and concentration [Q] for **a** Hg^{2+} **b** Pb^{2+} **c** Cd^{2+}

The linear range and the limit of detection (LOD) were calculated to study the detection performance of *Ag@GQDs* for different antibiotics and heavy metals; then, the results were compared with the previously reported Nanoprobes, and the results are listed in Tables 5, 6. It can be seen that our sensing system is superior to other fluorescent nanoprobes in detecting both antibiotics and toxic heavy metals. This is due to the reasons mentioned above. The produced *Ag@GQDs* nanocomposite provides active sites and a high surface area/volume ratio for the adsorption of antibiotic drugs. It can also alter the band gap, resulting in more fluorescence or saturation effect. The electrons that may be localized on *AgNPs* can be transferred between the two sensing nanomaterials when *Ag* and *GQDs* are mixed, leading to a sensing response. According to the justification, *Ag@GQDs* nanocomposite would rank among the greatest dual-functional nanosensors for the coming generation.

Table 4 Silver/graphene quantum dots quenched by Hg^{+2} , Pb^{+2} , and Cd^{+2}

Analyte	Linear regression equations	Correlation coefficient R^2	Linear range ppm	Limit of detection (LOD)
Hg^{+}	$I_0/I = 0.002[Q] + 1.1384$	0.9043	5–250	5 ppm
Pb^{+2}	$I_0/I = 0.0013[Q] + 1.0867$	0.9768	5–250	5 ppm
Cd^{+2}	$I_0/I = 0.0016 [Q] + 1.0997$	0.9533	5–250	5 ppm

Table 5 Comparison of sensing performance of variables nanoprobe for detecting antibiotics

Probe	Detected antibiotic	Method	Linear range (μM)	Limit of detection (LOD)	Year	Reference
N-GQDs	Oxytetracycline	Fluorescence	2–100 μM	100 nM	2020	Gao et al
GO	Oxytetracycline	Differential Pulse Voltammetry (DPV)	5–100 μM	6 nM	2016	Zhan et al
C-nanotubes	Oxytetracycline	Amperometry and adsorptive Stripping Voltammetry (AdSV)	Up to 8 μM	5.3 nM	2012	Nagles et al
CNT- $Fe_3O_4@SiO_2$	Tetracycline	Adsorptive stripping Differential pulse Voltammetry (AdSDPV)	400–460 μM	400 nM	2021	Amaral et al
Graphene-Au	Tetracycline	Cyclic Voltammetry (CV)	29–135 μM	16 nM	2021	Osikoya et al
Carbon	Oxytetracycline	<i>Square Wave Voltammetry</i> (SWV)	5–100 μM	415 nM	2021	Cánovas et al
SiO_2/Au	Erythromycin	Fluorescence		12 nM	2017	Zhang et al
Ag@GQDs	Oxytetracycline	Fluorescence	2–50 μM	2.7 nM		This work
	Erythromycin		3–60 μM	3.3 nM		

Table 6 Comparison of sensing performance of variables nanoprobe for detecting some toxic heavy metals such as Hg^{+2} , Pb^{+2} , and Cd^{+2}

Probe	Detected analyte	Method	Detection range	Year	Reference
Graphene oxide	Pb^{+2}	Electrochemical	Up to 10 ppm	2014	YangáTeoh
$AgNPs$	Hg^{+2}	Colorimetric	1–10 ppm	2018	Ban and Paul
$AgNPs$	Cd^{+2}	Electrochemical	1–10 ppm	2019	Pawar et al
$AuNPs/Graphene$	Cd^{+2}	Electrochemical	10 ppm	2017	Palisoc et al
$Alkanethiols/graphene$	Hg^{+2}	Colorimetric	10 ppm	2018	Amaral et al
$N,S\ CNDs$	Hg^{+2}	Fluorescence	0.064 ppm	2020	Sun et al
$CNDs$	Pb^{+}	Fluorescence	13.9 ppm	2010	Marcano et al
$CNDs$	Hg^{+2}	Fluorescence	0.3–1 ppm	2019	Desai et al
$CQDs$	Pb^{+}	Fluorescence	12.7 nM	2016	Liu et al
$N,S\ CNDs$	Hg^{+2}	Fluorescence	0.4–4 ppm	2014	Csavina et al
$CNDs$	Cd^{+2}	Fluorescence	0.29 nM	2018	Laali et al
$CNDs$	Hg^{+2}	Fluorescence	0–20 ppm	2015	Yu et al
$N-CNDs$	Pb^{+2}	Fluorescence	9.64 nM	2018	Bandi et al
$CQDs$	Hg^{+2}	Fluorescence	0.32 ppm	2018	Bano et al
$CQDs$	Pb^{+2}	Fluorescence	0.025 ppm	2017	Kumar et al
$Ag/GQDs$	Hg^{+2} , Cd^{+2} , Pb^{+2}	Fluorescence	5 ppm		This work

Conclusions

In summary, we have successfully developed a novel strategy to produce a Nanoprobe with dual functions and demonstrate their benefit in terms of simplicity, cost efficiency, and environmental friendliness. This work represents a synthesis of $Ag@GQDs$ by two different methods. One was green synthesis using new extracts of aquatic plants and seaweeds from *Edku & Marriott Lake*. It is essential to mention that $GQDs$ play the role of a protective Coating for $AgNPs$ surface by Connecting d orbitals of Ag^0 atoms or Ag^+ ions on the Ag nanoparticle's surface with the covalent electron pairs of COO and NH_2 group of $GQDs$. Therefore, it can prevent the aggregation of $AgNPs$, allowing $Ag@GQDs$ to be kept for a long time and to be stable in aqueous solutions.

The proposed nanosensors provide distinctive detection for both antibiotics and heavy metals. The detection is based on the nanocomposite's fluorescence quenching. The quenching percentages express the sensitivity of the synthesized $Ag@GQDs$ Nanoprobe, with *Oxytetracycline* and *Erythromycin* being the most sensitive antibiotics. The examined nanoprobe's duty includes not only the detection of antibiotics but also the identification of harmful heavy metals and their concentrations, such as Hg^{2+} , Pb^{2+} , and Cd^{2+} ions.

It is evident through the results that upon increasing the concentration, the fluorescence of the nanocomposite gradually decreases; this reflects that the present sensing system is highly sensitive. The current notion can be regarded as essential to developing the promising probe to be the ideal sensor.

Supplementary Information The online version contains supplementary material available at <https://doi.org/10.1007/s13204-023-02921-3>.

Acknowledgements The authors thank the central laboratory and laboratories of the National Institute of Oceanography and Fisheries for providing the required equipment to make the appropriate measurements.

Declarations

Conflict of interest The authors declare that they have no competing interests.

References

- Alexiev U, Farrens DL (2014) Fluorescence spectroscopy of rhodopsin's: insights and approaches. *Biochim Biophys Acta Bioenergy* 1837:694–709. <https://doi.org/10.1016/j.bbabi.2013.10.008>
- AlMasoud N, Alhaik H, Almutairi M, Houjak A, Hazazi K, Alhayek F, Awad MA (2021) Green nanotechnology synthesized silver nanoparticles: characterization and testing its antibacterial activity. *Green Process Synth* 10:518–528. <https://doi.org/10.1515/gps-2021-0048>
- Amaral EF, Da Silva DN, Silva MC, Pereira AC (2018) Self-assembled molecular films of alkanethiols on graphene for heavy metal

sensing. *J Phy Chem* 122:474–480. <https://doi.org/10.1021/acs.jpcc.7b09499>

- Amaral EF, Daniela N, Da S, Maria C, Arnaldo C (2021) Development of an electrochemical sensor based on nanocomposite of $Fe_3O_4@SiO_2$ and multiwalled carbon nanotubes for determination of tetracycline in real samples. *Electrochem* 2:251–263. <https://doi.org/10.3390/electrochem2020018>
- Badshah MA, Koh NY, Zia AW, Abbas N, Zahra Z, Saleem MW (2020) Recent developments in plasmonic nanostructures for metal-enhanced fluorescence-based biosensing. *J Nanomater* 10:1749. <https://doi.org/10.3390/nano10091749>
- Ban DK, Paul S (2018) Rapid colorimetric and spectroscopy-based sensing of heavy metal and cellular free oxygen radical by surface-functionalized silver nanoparticles. *J Appl Surf Sci* 458:245–251. <https://doi.org/10.1016/j.apsusc.2018.07.069>
- Bano D, Kumar V, Singh VK, Hasan SH (2018) Green synthesis of fluorescent carbon quantum dots for the detection of mercury (II) and glutathione. *New J Chem* 42(8):5814–5821
- Bandi R, Dadigala R, Gangapuram BR, Guttena V (2018) Green synthesis of highly fluorescent nitrogen-doped carbon dots from Lantana camara berries for effective detection of lead (II) and bioimaging. *J Photochem Photobiol B Biol* 178:330–338
- Bokare A, Nordlund D, Melendrez C, Robinson R, Keles O, Wolcott A, Erogbogbo F (2020) Surface functionality and formation mechanisms of carbon and graphene quantum dots. *Diam Relat Mater* 110:108101. <https://doi.org/10.1016/j.diamond.2020.108101>
- Briffa J, Emmanuel S, Sinagra E, Renald B (2020) Heavy metal pollution in the environment and their toxicological effects on humans. *J Heliyon* 6:e0469. <https://doi.org/10.1016/j.heliyon.2020.e04691>
- Buniamin I, Akhir RM, Asli NA, Khusaimi Z, Malek MF, Mahmood MR (2022) Nanotechnology applications in biomedical systems. *Curr Nanomater* 7(3):167–180
- Cánovas R, Nick S, Alexander LN, Van N, Karolien D (2021) Tetracycline antibiotics: elucidating the electrochemical fingerprint and oxidation pathway. *Chemosensors* 9:187. <https://doi.org/10.3390/chemosensors9070187>
- Chini MK, Kumar V, Javed A, Satapathi S (2019) Graphene quantum dots and carbon nanodots for the FRET-based detection of heavy metal ions. *Nano Struct Nano-Objects* 19:100347. <https://doi.org/10.1016/j.nanoso.2019.100347>
- Couture JL, Froehlich HE, Buck BH, Jeffery KR, Krause G, Morris JA Jr, Halpern BS (2021) Scenario analysis can guide aquaculture planning to meet sustainable future production goals. *J ICES Mar Sci* 78:821–831. <https://doi.org/10.1093/ICESJMS/FSAB012>
- Csavina J, Field J, Félix O, Corral-Avitia AY, Sáez AE, Betterton EA (2014) Effect of wind speed and relative humidity on atmospheric dust concentrations in semi-arid climates. *Sci Total Environ* 487:82–90
- Desai ML, Jha S, Basu H, Singhal RK, Park TJ, Kailasa SK (2019) Acid oxidation of muskmelon fruit for the fabrication of carbon dots with specific emission colors for recognition of Hg^{2+} ions and cell imaging. *ACS Omega* 4(21):19332–19340
- FAO (2020) The State of World Fisheries and Aquaculture 2020. Sustainability in action. Rome, 244 p. <https://doi.org/10.4060/ca9229en>
- Fernández L, Sebastian T, Anton X, Brión R, Daniel S, Peter J (2021) Lateral interactions and order-disorder phase transitions of metal phthalocyanines on Ag (111). *J Phy Chem C* 125:15623–15635. <https://doi.org/10.1021/acs.jpcc.1c03948>
- FuL M, Hsu JH, Shih MK, Hsieh CW, Ju WJ, Chen YW, Hou CY (2021) Process optimization of silver nanoparticle synthesis and its application in mercury detection. *Micromachines* 12:1123
- Gao R, Zhibin W, Li W, Jiao L, Yijun D, Zhihua X, Jun F, Yunshan L (2020) Green preparation of fluorescent nitrogen-doped carbon

- quantum dots for sensitive detection of oxytetracycline in environmental samples. *Nanomater* 10:1561. <https://doi.org/10.3390/nano10081561>
- Heinrich E (2021) The development and evaluation of extracellular vesicles as a biocompatible anti-infective drug delivery system
- Ho WJ, Liu JJ, Chen JC (2021) Characterization of plasmonic scattering, luminescent down-shifting, and metal-enhanced fluorescence and applications on silicon solar cells. *J Nanomater* 11:1013. <https://doi.org/10.3390/nano11041013>
- Juneau A, Hope TO, Malenfant J, Mesko M, McNeill J, Frenette M (2022) Methods to predict potential reagents in iridium-based photo redox catalysis calibrated with stern-volmer quenching rate constants. *ACS Catal* 12:2348–2356
- Kachel SR, Klein BP, Morbec JM, Schöniger M, Hutter M, Schmid M, Gottfried J (2020) Chemisorption and physisorption at the metal/organic interface: bond energies of naphthalene and azulene on coinage metal surfaces. *J Phy Chem C* 124:8257–8268. <https://doi.org/10.1021/acs.jpcc.0c00915>
- Kamakshi K, Silva JPB, Sekhar KC, Agostinho Moreira J, Almeida A, Pereira M, Gomes MJM (2018) Substrate temperature effect on microstructure, optical, and glucose sensing characteristics of pulsed laser deposited silver nanoparticles. *Plasmonics* 13(4):1235–1241
- Kauffman DR, Sorescu DC, Schofield DP, Allen BL, Jordan KD, Star A (2010) Understanding the sensor response of metal-decorated carbon nanotubes. *Nano Lett* 10(3):958–963
- Kumar A, Chowdhuri AR, Laha D, Mahto TK, Karmakar P, Sahu SK (2017) Green synthesis of carbon dots from *Ocimum sanctum* for effective fluorescent sensing of Pb^{2+} ions and live cell imaging. *Sens. Actuators B Chem* 242:679–686
- Kumar N, Chamoli P, Misra M, Manoj MK, Sharma A (2022) Advanced metal and carbon nanostructures for medical, drug delivery and bio-imaging applications. *Nanoscale* 14:3987–4017
- Laali K, Greves WJ, Correa-Smits SJ, Zwarycz AT, Bunge S, Borosky G, Manna A, Paulus A, Chanan-Khan A (2018) Novel fluorinated curcuminoids and their pyrazole and isoxazole derivatives: Synthesis, structural studies, Computational/Docking and in-vitro bioassay. *J Fluor Chem* 206:82–98
- Liu Y, Zhou Q, Li J, Lei M, Yan X (2016) Selective and sensitive chemo sensor for lead ions using fluorescent carbon dots prepared from chocolate by one-step hydrothermal method. *Sens. Actuators B Chem* 237:597–604
- Liu X, Wu W, Cui D, Chen X, Li W (2021) Functional micro-/nanomaterials for multiplexed bio detection. *J Adv Mater* 33:2004734. <https://doi.org/10.1002/adma.202004734>
- Mandal D, Gupta AN, Chandra A (2019) DNA-supported graphene quantum dots for Ag ion sensing. *Nanotechnology* 30(25):255501
- Marcano DC, Kosynkin DV, Berlin JM, Sinitskii A, Sun Z, Slesarev A, Tour JM (2010) Improved synthesis of graphene oxide. *ACS Nano* 4(8):4806–4814
- Mehwish HM, Rajoka MSR, Xiong Y, Cai H, Aadil RM, Mahmood Q, Zhu Q (2021) Green synthesis of a silver nanoparticle using *Moringaoleifera* seed and its applications for antimicrobial and sun-light mediated photocatalytic water detoxification. *J Environ Chem Eng* 9:105290. <https://doi.org/10.1016/j.jece.2021.105290>
- Mustapha T, Misni N, Ithnin NR, Daskum AM, Unyah NZ (2022) A review on plants and microorganisms mediated synthesis of silver nanoparticles, role of plants metabolites and applications. *Int J Environ Res Public Health* 19:674
- Nagles E, Alvarez P, ArancibiaMoya V, Baez M, Garretton V, EhrenfeldStolzenbach KN (2012) Amperometric and voltammetric determination of Oxytetracycline in trout salmonid muscle using multi-wall carbon nanotube, ionic liquid and gold nanoparticle film electrodes. *Int J Electro Chem Sci* 7:11745–11757
- Naresh V, Lee N (2021) A review on biosensors and recent development of nanostructured materials-enabled biosensors. *J Sens* 21:1109. <https://doi.org/10.3390/s21041109>
- Osikoya A, Poomani G (2021) Electrochemical detection of tetracycline on highly sensitive benzene sourced CVD graphene-gold nanoparticles nanointerfaces. *J Electroanal* 33:412–420. <https://doi.org/10.1002/elan.202060230>
- Palisoc ST, Valeza N, Natividad MT (2017) Fabrication of an effective gold nanoparticle/graphene/Nafion-modified glassy carbon electrode for high sensitive detection of trace Cd^{2+} , Pb^{2+} and Cu^{2+} in tobacco and tobacco products. *Int J Electrochem Sci* 12:3859–3872. <https://doi.org/10.20964/2017.05.14>
- Pawar AV, Kanapally SS, Kadam KD, Patil SL, Dongle VS, Jadhav SA, Dongale TD (2019) MemSens: a new detection method for heavy metals based on silver nanoparticle-assisted memristive switching principle. *J Mater Sci: Mater Electron* 30:11383–11394. <https://doi.org/10.1007/s10854-019-01487-7>
- Peng B, Chen L, Que C, Yang K, Deng F, Deng X, Wu M (2016) Adsorption of antibiotics on graphene and biochar in aqueous solutions induced by π - π interactions. *Sci Reports* 6(1):1–10
- Perera D, Abeywickrama A, Zen F, Colavita PE, Jayasundara DR (2018) Evolution of oxygen functionalities in graphene oxide and its impact on structure and exfoliation: an oxidation time-based study. *Mater Chem Phys* 220:417–425
- Quyen TTB, Nhon NH, Duong TNT, My NNT, Thien DVH, Thanh LHV (2021) Rapid and simple synthesis of graphene quantum dots/Ag nanocomposites and its application for glucose detection by photoluminescence spectroscopy. *Inter J Sci Eng Sci* 5(6):1–5
- Rajeev YN, Venkatarao K, Kumar BN, Kumar LB, Cole S (2022) Structural, morphological and luminescent studies on Sm^{3+} doped strontium tin phosphate nanopowder. *Mater Today: Proc* 49:554. <https://doi.org/10.1016/j.matpr.2021.12.554>
- Satapathi S, Vishal K, Mrinmoy K, Rajesh B, Krishna K, Amitava P (2018) Highly sensitive detection and removal of mercury ion using a multimodal nanosensor. *Nano Struct Nano-Objects* 16:120–126. <https://doi.org/10.1016/j.nanoso.2018.05.006>
- Seku K, Kumar KK, Narasimha G, Reddy GB (2022) Chapter 7: Biomediated synthesis of silver nanoparticles via microwave-assisted technique and their biological applications. *Green synthesis of silver nanomaterials*. Elsevier, pp 149–188
- Shao Y, Wang Y, Yuan Y, Xie Y (2021) A systematic review on antibiotics misuse in livestock and aquaculture and regulation implications in China. *Sci Total Environ* 798:149205. <https://doi.org/10.1016/j.scitotenv.2021.149205>
- Sharma V, Pranav T, Shaikh M (2017) Sustainable carbon dots: recent advances in green carbon dots for sensing and bioimaging. *J Mater Chem B* 5:8904–8924. <https://doi.org/10.1039/C7TB02484C>
- Sharma A, Majdinasab M, Khan R, Li Z, Hayat A, Marty JL (2021) Nanomaterials in fluorescence-based biosensors: Defining key roles. *Nano-Struct Nano-Objects* 27:10077. <https://doi.org/10.1016/j.nanoso.2021.100774>
- Sun D, Liu T, Wang C, Yang L, Yang S, Zhuo K (2020) Hydrothermal synthesis of fluorescent carbon dots from gardenia fruit for sensitive on-off-on detection of Hg^{2+} and cysteine. *Spectrochim Acta A Mol Biomol Spectrosc* 240:118598
- Tang H, Li Y, Ye H, Hu F, Gao C, Tao L, Zhang G (2019) High-performance humidity sensor using Schottky-contacted SnS nanoflakes for noncontact healthcare monitoring. *Nano Technol* 31(5):055501
- Tiseo K, Huber L, Gilbert M, Robinson TP, Van Boeckel TP (2020) Global trends in antimicrobial use in food animals from 2017 to 2030. *J Antibiotics* 9:918. <https://doi.org/10.3390/antibiotic9120918>
- Varghese AK, Tamil PP, Rugmini R, Shiva PM, Kamakshi K, Sekhar KC (2020) Green synthesized Ag nanoparticles for bio-sensing and photocatalytic applications. *ACS Omega* 5(22):13123–13129

- Vinay SP, Nagarju G, Chandrappa CP, Chandrasekhar N (2019) Enhanced photocatalysis, photoluminescence, and antibacterial activities of nanosize Ag: green synthesized via *Rauvolfia tetraphylla* (devil pepper). *SN Appl Sci* 1(5):1–14
- YangáTeoh W (2014) Graphene oxide-based electrochemical sensor: a platform for ultrasensitive detection of heavy metal ions. *RSC Adv* 4:24653–24657. <https://doi.org/10.1039/c4ra02247e>
- Yu J, Song N, Zhang YK, Zhong SX, Wang AJ, Chen J (2015) Green preparation of carbon dots by Jinhua bergamot for sensitive and selective fluorescent detection of Hg^{2+} and Fe^{3+} . *Sens Actuators B Chem* 214:29–35
- Zhan X, Hu G, Wagberg T, Zhan S, Xu H, Zhou P (2016) Electrochemical aptasensor for tetracycline using a screen-printed carbon electrode modified with an alginate film containing reduced graphene oxide and magnetite (Fe_3O_4) nanoparticles. *Microchim Acta* 183:723–729. <https://doi.org/10.1007/s00604-015-1718-y>
- Zhang A, Zhang J, Fang Y (2008) Photoluminescence from colloidal silver nanoparticles. *J Lumin* 128(10):1635–1640
- Zhang Y, Zhou Z, Zheng J, Li H, Cui J, Liu S, Li C (2017) SiO₂-MIP core-shell nanoparticles containing gold nanoclusters for sensitive fluorescence detection of the antibiotic Erythromycin. *Microchim Acta* 148:2241–2248. <https://doi.org/10.1007/s00604-017-2216-1>
- Zhang L, Liu L, Wang J, Niu M, Zhang C, Yu S, Yang Y (2020) Functionalized silver nanoparticles with graphene quantum dots shell layer for effective antibacterial action. *J Nanoparticle Res* 22(5):1–12

Publisher's Note Springer Nature remains neutral with regard to jurisdictional claims in published maps and institutional affiliations.

Springer Nature or its licensor (e.g. a society or other partner) holds exclusive rights to this article under a publishing agreement with the author(s) or other rightsholder(s); author self-archiving of the accepted manuscript version of this article is solely governed by the terms of such publishing agreement and applicable law.